Acta Mech 226, 3565–3586 (2015)
DOI 10.1007/s00707-015-1390-7

ORIGINAL PAPER

S. O. Gajbhiye · S. P. Singh

Vibration characteristics of open- and capped-end single-walled carbon nanotubes using multi-scale analysis technique incorporating Tersoff–Brenner potential

Received: 2 December 2014 / Revised: 3 May 2015 / Published online: 26 June 2015

Abstract This research work addresses questions on the vibration characteristics of single-walled carbon nanotubes (SWCNTs) using multi-scale analysis. Atomistic finite element method (AFEM) is one such multi-scale technique where sequential mode is used to transfer information between two length scales to model and simulate the nanostructures at continuum level. This method is used to investigate the vibration characteristics of SWCNTs. Open- and capped-end armchair and zigzag nanotubes are considered with clamped-free and clamped–clamped boundary conditions. The dependence of vibration characteristic of SWCNTs on their length, diameter and atomic structure is also demonstrated. The body interatomic Tersoff–Brenner (TB) potential is used to represent the energy between two carbon atoms. Based on the TB potential, a new set of force constant parameters is established for carbon nanotubes and presented in this paper. Molecular and structural mechanics analogy is used to find the equivalent geometric and elastic properties of the space frame element to represent the carbon–carbon bond. To validate the vibration results of AFEM incorporating the proposed new set of force constants, molecular dynamics simulation is also carried out on the same structure of carbon nanotube, and it is found that they are in good agreement with each other.

1 Introduction

Single-walled carbon nanotubes (SWCNTs) are much stronger than steel at one-sixth its weight. This makes SWCNTs a potentially highly valued reinforcing material to strengthen composite materials. These composite materials can then be used in the development of high strength requirement components for use in vehicles and aerospace industries. Carbon nanotubes (CNTs) also have extraordinary electronic properties and, depending on their structure, can be either metallic or semiconducting. Thus, some nanotubes have a conductivity higher than that of copper, while others behave like silicon. Poncharal et al. [1] induced the static and dynamic mechanical deflections in cantilevered multi-walled carbon nanotubes electrically in a transmission electron microscope and resonantly excited the nanotubes at the fundamental frequencies and higher harmonics. They applied this method to a nanobalance for nanoscopic particles and to a Kelvin probe based on nanotubes. The nanotubes also have potential application in actuators, sensors, paints and coatings, biological, flat-panel displays, scanning probe microscope, etc. In all these applications, the vibration characteristics of nanotubes are of extreme importance and needed beforehand. These characteristics of SWCNTs are investigated in this paper using a multi-scale analysis technique.

Shen et al. [2–4] used an energy approach in the framework of molecular mechanics to evaluate the local and global deformations of a single-walled and multi-walled carbon nanotube. They proposed a replacement

S. O. Gajbhiye (✉) · S. P. Singh
Design Research Laboratory, Department of Mechanical Engineering, Indian Institute of Technology Delhi, Hauz Khas, New Delhi 110016, India
E-mail: sachin.iitdelhi2011@gmail.com
Tel.: +91-11-26591136

method to derive the corresponding expressions for the cases of more than two walls. They have also analyzed the equilibrium structure and strain energy per atom of armchair and zigzag SWCNTs by developing a simple force-field-based atomistic model. Wang et al. [5] presented a Timoshenko beam model for vibration analysis of multi-walled carbon nanotubes. The differential quadrature method is used to solve the governing Timoshenko equations for CNTs of aspect ratio and boundary conditions. By comparing the results based on the Timoshenko and Euler beam theories, they showed that the Euler beam theory overpredicted the frequencies significantly. Sun et al. [6] studied the vibration characteristics of multi-walled carbon nanotubes with initial axial loading based on Donnell equations and discussed the effect on initial axial stress and the effect of van der Walls forces. They showed that the resonant frequencies are related to the tension or compression forms of initial axial stress, which increases with an increase in axial tensile stress, and decreases with an increase in axial compressive stress. Gupta et al. [7] studied the axial, torsional and radial breathing mode vibrations of free–free unstressed SWCNTs of different chirality using the MM3 potential. They found that for axial and torsional vibrations, frequencies of the second and third modes of SWCNTs are equal to twice and thrice that of the corresponding first mode, respectively.

Georgantzinos et al. [8,9] presented a linear spring-based element formulation for computation of vibrational characteristics of single-walled and multi-walled carbon nanotubes. They developed a three-dimensional nanoscale element and corresponding element equations for the numerical treatment of the dynamic behavior of SWCNTs. Ke et al. [10] studied the nonlinear free vibration of embedded double-walled carbon nanotubes based on Eringen's nonlocal elasticity theory and von Kármán geometric nonlinearity. They considered the effect of transverse shear deformation and rotary inertia in their formulation and described the surrounding elastic medium as the Winkler model characterized by the spring. They used Hamilton's principle to derive the governing equations and boundary conditions and used the differential quadrature method to discretize the nonlinear governing equations. Using this formulation, they investigated the influence of nonlocal parameters, length of the tubes, spring constants and the end supports on the nonlinear free-vibration characteristics of double-walled carbon nanotube. Sakhaee-Pour et al. [11] used a finite element approach to study vibration behavior of SWCNTs of different length and diameter. They used beam and mass elements to represent carbon–carbon bond and carbon atom, respectively, and calculated the elastic properties of beam by considering mechanical characteristics of the covalent bonds between the carbon atoms in the hexagonal lattice. Chowdhury et al. [12] investigated the vibration properties of zigzag and armchair SWCNTs using molecular mechanics approach. They used universal force-field potential for the molecular mechanics approach and found that the natural frequency decreases as the aspect ratio increases.

Arghavan et al. [13] presented a detailed numerical study on the free and forced vibrations of SWCNTs. They analyzed zigzag and armchair configurations of the carbon nanotubes for clamped-free and clamped–clamped boundary conditions and obtained their natural frequencies and corresponding mode shapes. Aydogdu et al. [14] studied the axial vibration of SWCNT embedded in an elastic medium using nonlocal elasticity theory. They used nonlocal constitutive equations of Eringen in their formulations and discussed the effect of stiffness of the elastic medium, boundary conditions and nonlocal parameters on the axial vibration of nanotubes. Ansari et al. [15] investigated the vibrational characteristics of SWCNTs based on gradient elasticity theories. They established the theoretical formulations based upon Euler–Bernoulli and Timoshenko beam theories and validated their model by conducting molecular dynamics (MD) simulations for an armchair SWCNT. Ghavanloo et al. [16] developed an anisotropic elastic shell model to study the vibration characteristics of chiral SWCNTs. They presented the analytical solution by using the Flügge shell theory and complex method and investigated the influence of the externally applied mid-face axial force and torque on longitudinal, radial and torsional frequencies of SWCNTs.

Although there are several papers available in the literature on carbon nanotubes, no work exists on the vibration analysis of SWCNTs using an atomistic finite element method (AFEM) incorporating the multi-body interatomic Tersoff–Brenner (TB) potential, which is more accurate to describe the carbon–carbon bond. In the papers available in the literature, assumptions are made on the selection of the interatomic potential based on the simplicity of formulation and computational ease. Also, in most of the articles, the force constant parameters are directly taken from the AMBER [17]. This issue is addressed in this paper in detail, and an AFEM incorporating TB potential [18,19] is proposed to investigate the vibration characteristics of SWCNTs. Based on the TB potential, a new set of force constant parameters is established for the carbon nanotubes. Using these force constant parameters, the equivalent elastic and geometric properties of the carbon–carbon bond of SWCNTs are derived which are consistent with the material constitutive relation. The AFEM is one of the multi-scale simulation techniques where information at molecular state is used to simulate the nanostructures at continuum level. This approach uses continuum or structural elements to represent nanostructures at continuum

level, and the equivalent material properties of these elements are derived by the interatomic potentials between atoms. To represent a carbon nanotube at continuum level, space frame and mass elements are used in this paper. The space frame element represents the carbon–carbon bond, while the mass element represents a carbon atom. SWCNTs of different length are considered, and the natural frequencies are calculated for clamped-free and clamped–clamped boundary conditions. Before using the proposed AFEM to investigate the dynamic characteristics of SWCNTs, it is validated using MD simulation results.

2 Schematics and geometric description of SWCNT

A SWCNT can be viewed as a graphene sheet that has been rolled into a tube as shown in Fig. 1. Graphite assumes the form of a two-dimensional sheet of carbon atoms arranged in a hexagonal array as shown in Fig. 2 [20]. The atomic structure of a carbon nanotube can be described by its chirality. The two factors which define the chirality of a nanotube are the chiral vector $\vec{C}_h$ and the chiral angle θ. The chiral vector can be described by the following equation:

$$\vec{C}_h = n\vec{a}_1 + m\vec{a}_2, \tag{1}$$

where the integers (n, m) are the number of steps along the zigzag carbon bonds of the hexagonal lattice and $\vec{a}_1$ and $\vec{a}_2$ are unit vectors.

The chiral angle is calculated as

$$\theta = \cos^{-1}\left[(2n+m)/2\sqrt{(n^2+nm+m^2)}\right]. \tag{2}$$

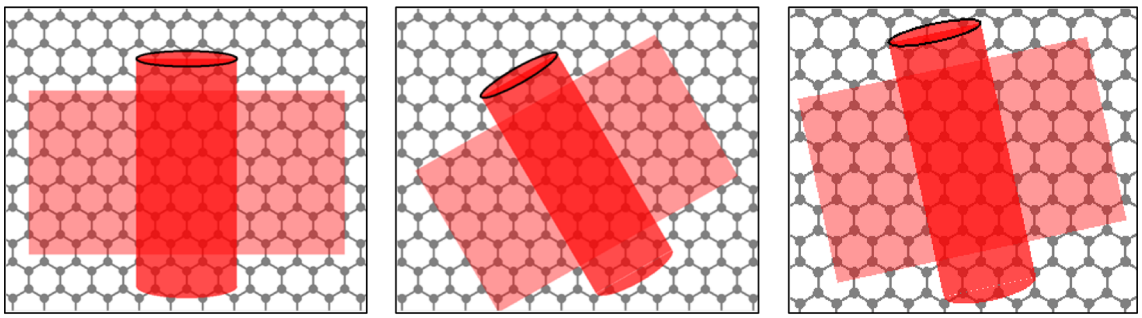

Fig. 1 Schematic view of different kinds of nanotubes: **a** zigzag, **b** armchair and **c** chiral

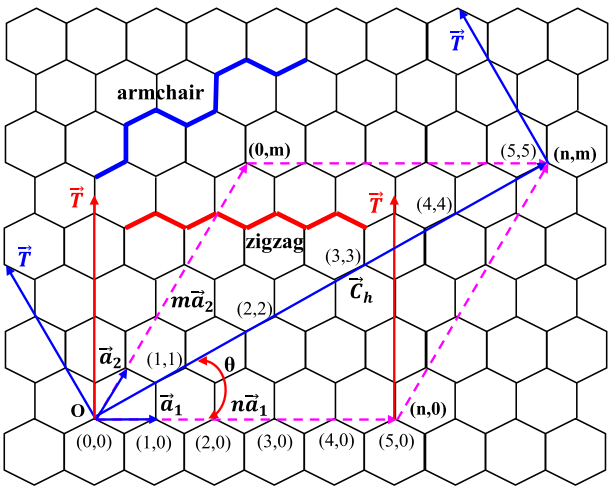

Fig. 2 Graphene sheet of a single-walled carbon nanotube

The zigzag nanotube is denoted by $(n, 0)$ as shown in Fig. 1a, while the armchair nanotube is denoted by (n, n) as shown in Fig. 1b. Apart from zigzag and armchair, a nanotube with some different chirality is denoted by (n, m) as shown in Fig. 1c. The chiral angle for the armchair nanotube is 30°, while for the zigzag nanotube it is zero degrees. The nanotube radius R is given as [20]

$$R = \vec{C}_h/2\pi = a_{c-c}\sqrt{3(n^2 + nm + m^2)}/2\pi, \tag{3}$$

where a_{c-c} is the distance between two neighboring carbon atoms.

The chiral vector $\vec{C}_h$ and the translational vector $\vec{T}$ define the ideal rectangular cutting area of a graphene sheet, as shown in Fig. 2. The translational vector $\vec{T}$ is defined as [20]

$$\vec{T} = [(2m + n)/w]\,\vec{a}_1 - [(2n + m)/w]\,\vec{a}_2, \tag{4}$$

where w is the greatest common divisor of $(2m + n)$ and $(2n + m)$.

3 Atomistic finite element method

3.1 Molecular and structural mechanics of SWCNTs

From the molecular mechanics point of view, a SWCNT can be considered as a large molecule consisting of carbon atoms and bonds to connect those atoms. The atomic nuclei can be regarded as material points, and their motions are regulated by a force field, which is generated by electron–nucleus interactions and nucleus–nucleus interactions [21]. Molecular mechanics, which is based on the Born–Oppenheimer approximation, expresses the system energy only as a function of the nuclear positions and ignores the electronic structure. Usually, the force field is expressed in the form of steric potential energy and it depends solely on the relative positions of the nuclei constituting the molecule. The general expression of total potential energy is a sum of energies due to bonded or valence interactions and nonbonded interactions [21,22], as shown in Eq. (5),

$$V = \sum V_r + \sum V_\theta + \sum V_\varphi + \sum V_\omega + \sum V_{\text{vdw}} \tag{5}$$

where V_r is for a bond stretch interaction, V_θ for a bond angle bending, V_φ for a dihedral angle torsion, V_ω for an improper (out-of-plane) torsion, and V_{vdw} for a nonbonded van der Waals interaction. All these energy terms are shown in Fig. 3 [23].

There are several potential functions available to describe the carbon–carbon bond [24], viz. harmonic function, cubic anharmonic function, quartic function, Morse function, TB potential function. Among them, the TB potential function [18,19] is the most accurate one and widely used in MD simulations. This potential function is used in this paper to describe the carbon–carbon bond and to calculate the bond stretching and bond angle bending force constant.

In the TB potential, the energy between atom i and j is expressed as [25]

$$V(r_{ij}) = \left(\frac{D^{(e)}}{S-1}\mathrm{e}^{-\sqrt{2S}\beta(r-R^{(e)})}f_c(r)\right) - \left(\frac{\frac{D^{(e)}S}{S-1}\mathrm{e}^{-\sqrt{2/S}\beta(r-R^{(e)})}f_c(r)}{\left(1 + 2a_0 f_c(r)\left[1 + \frac{c_0^2}{d_0^2} - \frac{c_0^2}{d_0^2+(1+\cos\theta_{ijk})^2}\right]\right)^{\delta}}\right), \tag{6}$$

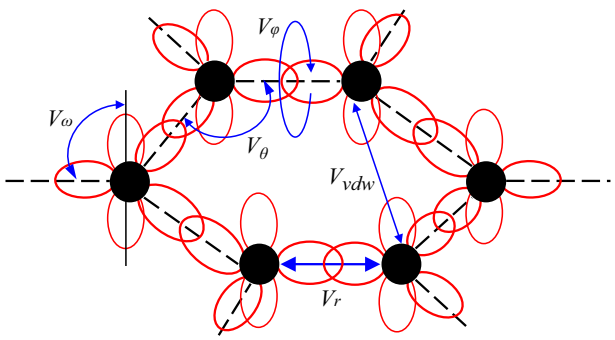

Fig. 3 Energy terms of bonded and nonbonded interaction

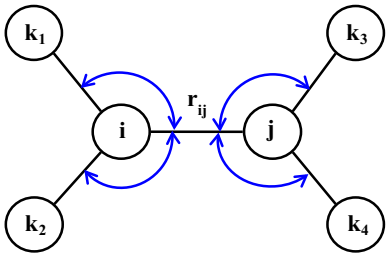

Fig. 4 Part of nanotube with angle bending

Table 1 Parameters of Tersoff–Brenner potential

$D^{(e)}$ (eV)	S	β (Å^{-1})	$R^{(e)}$ (Å)	$R^{(1)}$ (Å)	$R^{(2)}$ (Å)	δ	a_0	c_0	d_0
6	1.22	2.1	1.390	1.7	2	0.5	0.00020813	330	3.5

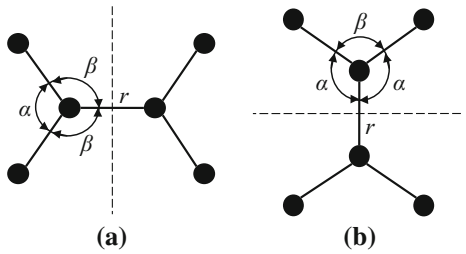

Fig. 5 Schematic illustration of angles in **a** an armchair CNT and **b** zigzag CNT

where r_{ij} is the distance between atoms i and j (Fig. 4), which is equal to the bond length at initial equilibrium configuration. The value of the cutoff function $f_c(r)$ is assumed as 1, which is generally used to reduce the computation time by limiting the range of the potential and to include only the first neighbor shell of carbon atoms.

To calculate the bond stretching and bond angle bending force constants of the carbon–carbon bond, the part of the nanotube as shown in Fig. 4 is considered. Deriving from Eq. (6), the relation between force and bond length variation [Eq. (7)], as well as the relation between moment and bond angle variation [Eq. (8)], can be written as

$$F(r) = \left(\frac{\sqrt{2S}\beta f_c(r) D^{(e)} \mathrm{e}^{-\sqrt{2/S}\beta(r-R^{(e)})}}{\left(1 + 2a_0 f_c(r)\left[1 + \frac{c_0^2}{d_0^2} - \frac{c_0^2}{d_0^2+(1+\cos\theta_{ijk})^2}\right]\right)^{\delta} (S-1)} \right) - \left(\frac{\sqrt{2S}\beta f_c(r) D^{(e)} \mathrm{e}^{-\sqrt{2S}\beta(r-R^{(e)})}}{S-1} \right), \tag{7}$$

$$M(\theta) = \frac{4D^{(e)} S\delta a_0 c_0^2 f_c^2(r) \mathrm{e}^{-\sqrt{2/S}\beta(r-R^{(e)})} \sin\theta_{ijk}(1+\cos\theta_{ijk})}{\left(1 + 2a_0 f_c(r)\left[1 + \frac{c_0^2}{d_0^2} - \frac{c_0^2}{d_0^2+(1+\cos\theta_{ijk})^2}\right]\right)^{\delta+1} (S-1)(d_0^2 + (1+\cos\theta_{ijk})^2)^2}. \tag{8}$$

All the parameters used in the TB potential are listed in Table 1 [19]. With this set of parameters, the bond length is taken as 0.145 nm.

In a graphene sheet, the value of θ_{ijk} (the angle between bonds $i-j$ and $i-k$ at equilibrium position) in Eq. (7) is 120°, whereas in carbon nanotubes, the actual angle is dependent on the chirality of the tube. Ye et al. [26] expressed the angle α and β for armchair nanotubes (Fig. 5a) based on *ab initio* calculations as $\alpha \approx 2\pi/3$ and $\beta = \pi - \cos^{-1}[0.5\cos(\pi/2n_1)]$. Similarly, the expressions of the angles α and β for zigzag nanotubes (Fig. 5b) are [26] $\alpha \approx 2\pi/3$ and $\beta = \cos^{-1}[0.25 - 0.75\cos(\pi/n_1)]$. The angle β varies between 115° and 120° in most of the armchair and zigzag nanotubes at equilibrium stable configuration. As the diameter of the nanotube increases, the angle β also increases and reaches close to 120°. In case of higher chirality nanotube, both armchair and zigzag, the difference between the angles α and β is negligible.

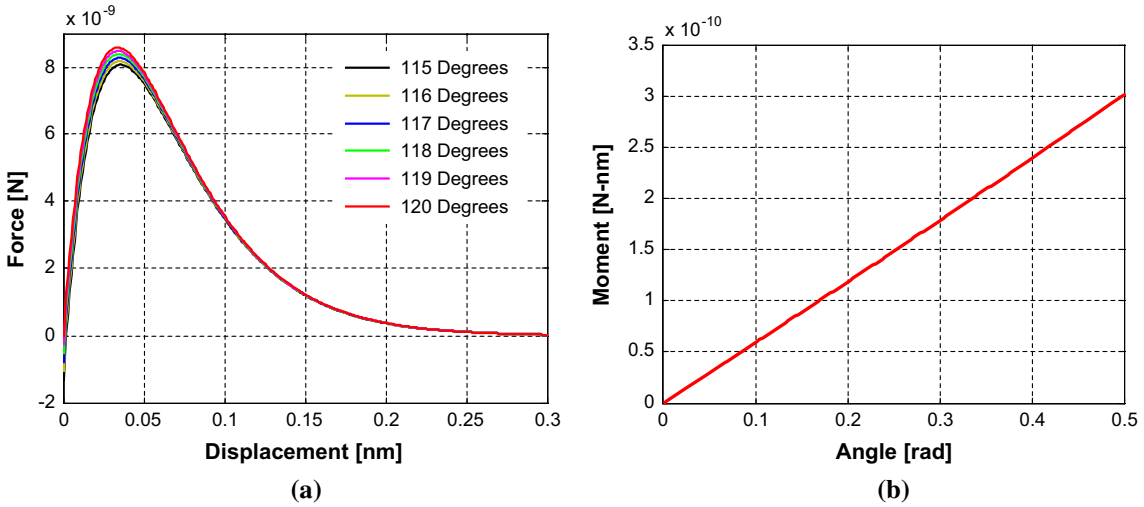

Fig. 6 **a** Force versus displacement curve and **b** moment versus angle variation curve of C–C bond

The force versus bond length variation (Eq. (7)) and moment and bond angle variation (Eq. (8)) are plotted in Fig. 6a, b, respectively, using the parameters listed in Table 1.

A relationship between the structural mechanics parameters *EA*, *EI* and *GJ* and the molecular mechanics parameters k_r, k_θ and k_τ is as follows [21]:

$$\frac{EA}{L} = k_r, \quad \frac{EI}{L} = k_\theta, \quad \frac{GJ}{L} = k_\tau. \tag{9}$$

Equation (9) is the foundation of applying the theory of structural mechanics to the modeling of nanotubes or other similar structures. k_r, k_θ and k_τ are the force constants which come from the atomistic scale, whereas *EA*, *EI* and *GJ* represent the properties of the continuum scale. k_r, k_θ and k_τ are the bond stretching force constant, bond angle bending force constant and torsional resistance, respectively. E, G, I, L and J are the modulus of elasticity, modulus of rigidity, moment of inertia, length of beam and polar moment of inertia. The expressions for the force constants k_r, k_θ and k_τ have been used which give consistent values of the moduli, while retaining the theoretical constraint limits on Poisson's ratio. This approach was first used by Adhikari et al. [27] and has been implemented here with some modifications with the purpose to find the Poisson's ratio and the thickness of the carbon–carbon bond [28,29],

$$k_\theta = \frac{k_r d^2}{16}\left[\frac{448k_\tau L^2 + 384k_\tau L^2\nu + 9d^4k_r + 9d^4k_r\nu}{112k_\tau L^2 + 96k_\tau L^2\nu + 9d^4k_r + 9d^4k_r\nu}\right], \tag{10}$$

where ν is the Poisson's ratio of the space frame element material and d is the diameter of circular cross-section of the carbon–carbon bond in the SWCNT.

In the literature, the commonly used values for the force-field parameters of Eq. (23) are taken from AMBER [17]. The values of these parameters as listed in AMBER are $k_r = 6.52E^{-7}$ N/nm, $k_\theta = 8.76E^{-10}$ N-nm/rad^2 and $k_\tau = 2.78E^{-10}$ N-nm/rad^2. Chang et al. [23] used a different set of these parameters which are $k_r = 7.42E^{-7}$ N/nm, $k_\theta = 1.42E^{-9}$ N-nm/rad^2 and $k_\tau = 0.15E^{-9}$ N-nm/rad^2. Lu et al. [30] have devised another set of these parameters based on the Morse potential which are $k_r = 7.86E^{-7}$ N/nm and $k_\theta = 0.901E^{-9}$ N-nm/rad^2. All these sets of parameters have significant difference among them that will reflect in the overall results.

In this paper, the values of bond stretching force constant (k_r) and bond angle bending force constant (k_θ) are derived directly from the TB potential. The stiffness k_r is calculated based on the slope of the force versus displacement curve as shown in Fig. 6a which is approximately linear below 5 % strain for a variation of bond angle ranging from 115° to 120°. The slope of this curve within the range of 5 % strain is taken as bond stretching force constant (k_r). Also, as the diameter of the nanotube increases, the difference between the angles α and β decreases ($\beta \approx \alpha = 120°$). So, for higher chirality nanotubes and small strain applications (eigenvalue analysis), this small difference between angles can also be neglected when computing the value of the stretching force constant. The bond angle bending force constant (k_θ) is calculated based on the slope of the

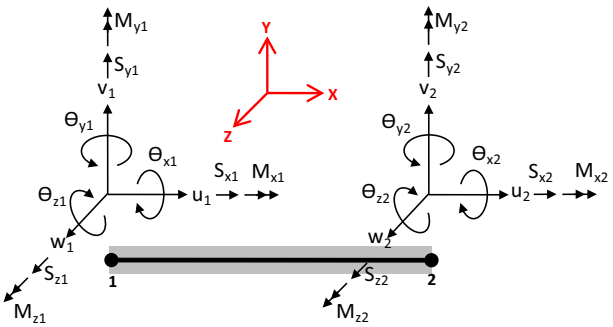

Fig. 7 Space frame element with 6 degrees of freedom per node

moment versus angle curve as shown in Fig. 6b which shows approximately linear behavior below 0.43 radians angle variation. The computed values of these force constants from the TB potential are $k_r = 6E^{-7}$ N/nm and $k_\theta = 6E^{-10}$ N-nm/rad^2. The value of torsional resistance is taken as $k_\tau = 1.5E^{-10}$ N-nm/rad^2 [23]. This proposed set of force constants is used to solve Eq. (10).

After imposing the isotropic material condition $d^2k_r = 16k_\tau(1+\nu)$ for the equivalent C–C bond element to constrain Eq. (10) using the Marquardt algorithm, the optimized value of the diameter (d) and Poisson's ratio (ν) is 0.0716 nm and 0.28, respectively. By using the value of the optimized equivalent diameter, force-field parameters and Eq. (9), the computed values of Young's modulus and shear modulus are 21.607 and 8.44 TPa, respectively. These equivalent geometric and elastic properties are used to define the space frame element (beam) to represent a carbon–carbon bond of the SWCNT. The derived equivalent Young's modulus, shear modulus and Poisson's ratio of the carbon–carbon bond satisfy the material constitutive relation.

3.2 Finite element formulation and modeling procedure of SWCNTs

The space frame element implemented in the formulation is shown in Fig. 7. It is a three-dimensional 2-noded element with 6 degrees of freedom at each node, three translations and three rotations. The formulation of the element stiffness matrix for this element comprises contributions from one axial, one torsional and two bending actions, one about each of two orthogonal local axes. The contributions from axial and torsional effects to the element stiffness matrix are formulated in the conventional way, whereas the bending contributions are as per Timoshenko beam theory. Different terms used in Fig. 7 are listed below. All these terms are at node 1 and node 2, respectively. These terms include six components of displacement, the six components of rotation, the six components of force and the six components of moment:

(u_1, u_2), (v_1, v_2) and (w_1, w_2) are displacements in X, Y and Z direction,
$(\Theta_{x1}, \Theta_{x2})$, $(\Theta_{y1}, \Theta_{y2})$ and $(\Theta_{z1}, \Theta_{z2})$ are rotations about X, Y and Z axis,
(S_{x1}, S_{x2}), (S_{y1}, S_{y2}) and (S_{z1}, S_{z2}) are forces along X, Y and Z axis and
(M_{x1}, M_{x2}), (M_{y1}, M_{y2}) and (M_{z1}, M_{z2}) are moments about X, Y and Z axis, respectively.

A three-dimensional mass element is used to represent and simulate the mass of each carbon atom (m_c= 1.9943E^{-26} kg). It is positioned at each end of the space frame element as a lumped mass. The finite element details of the space frame and mass element can be found in [21,25,31]. The commercial finite element code ANSYS is used to model and compute the eigenvalue problem of SWCNTs. Beam188 with 6 degrees of freedom at each node is used to represent a carbon–carbon bond which is equivalent to the space frame element. The mass of a carbon atom is represented by a MASS21 element at the joint of each space frame element. Once the finite element model is created using mass and beam element, then element matrices are assembled as global mass and stiffness matrices $[M]$ and $[K]$, respectively. The general formulation of the differential equation governing free undamped vibration can be written as

$$[M]\,\ddot{x} + [K]\,x = 0, \tag{11}$$

where $[M]$ and $[K]$ are the symmetric $m \times m$ mass and stiffness matrices, respectively. x is the m-dimensional displacement column vector composed of all global degrees of freedom. From Eq. (11), the standard undamped eigenvalue equation is defined as

$$\left([K] - \omega^2\,[M]\right)\{\psi\} = \{0\}\,. \tag{12}$$

Table 2 Natural frequencies of a zigzag (8, 0) SWCNT with aspect ratio 9.31

Mode no.	Natural frequency (THz)		
	Molecular dynamics simulation	Atomistic FEM (proposed)	Reference [11]
1	0.050	0.053	0.072
2	0.050	0.053	0.072
3	0.289	0.308	0.421
4	0.289	0.308	0.421
5	0.410	0.409	0.628
6	0.595	0.672	0.882
7	0.729	0.779	1.07
8	0.729	0.779	1.07
9	1.219	1.225	1.87
10	1.256	1.355	1.87

A classical Block Lanczos algorithm implemented in ANSYS is used to solve Eq. (12), and the frequencies of free vibrations as well as the corresponding mode shapes are obtained.

Armchair and zigzag SWCNTs with open- and capped-end configurations are considered to investigate its vibration characteristics using AFEM and the proposed new set of force constants. While simulating SWCNTs, two boundary conditions are considered. In the first case, one end is assumed as fixed and the other end is free, termed as clamped free. In the second case, both ends are assumed as fixed, termed as clamped–clamped. The results and discussions are organized as follows. The vibration characteristics of open-end zigzag and armchair SWCNTs are investigated, and its dependence on length, diameter and atomic structure is discussed individually. Further, the vibration characteristics of capped armchair and zigzag SWCNTs are also investigated and compared with the open-end SWCNTs of same chirality.

4 Results and discussion

MD simulation with the COMPASS (condensed-phase optimized molecular potentials for atomistic simulation studies) interatomic potential [32] is carried out on a zigzag (8, 0) SWCNT for the aspect ratio of 9.31 with a clamped-free boundary condition to validate the results of the proposed new set of force constants and the AFEM. The results of the proposed method are also compared with the results available in the literature. The natural frequencies of the SWCNT computed through MD simulation, the proposed AFEM and those available in the literature are tabulated in Table 2. It can be seen that the natural frequencies predicted by Sakhaee-Pour et al. [11] are slightly higher than those computed by MD simulation, whereas the results of the proposed AFEM are much closer to the MD simulation results. Hence, the established new set of force constant parameters and the AFEM are validated to be used further to investigate the vibration characteristics of SWCNTs.

4.1 Dependence on the length

The zigzag SWCNTs with chirality (6, 0), (7, 0), (8, 0), (9, 0) and (10, 0) are considered in this study and solved for clamped-free and clamped–clamped boundary conditions. The length of the zigzag nanotubes is varied from 24.65 to 102.95 Å. Similarly, the armchair SWCNTs with chirality (6, 6), (7, 7), (8, 8), (9, 9) and (10, 10) are considered, and the length is varied from 33.905 to 124.32 Å.

4.1.1 Clamped-free zigzag SWCNTs

Figure 8 shows the variation of the first four natural frequencies of zigzag SWCNTs with respect to the length, for clamped-free boundary condition. The first and second natural frequencies are the repeated eigenvalues of the characteristic equation of zigzag SWCNTs. It is observed that all of the natural frequencies decrease with the increase in length of the nanotube. The rate of decrease in natural frequencies is larger near the lower length are becomes smaller with the increase in length. The third natural frequencies of all the considered nanotubes are very close to each other for the length of 24.65 and 33.35 Å and become separated at larger length. For the same length (24.65 Å), the fourth natural frequencies of the nanotubes (10, 0) and (6, 0) nearly coincides.

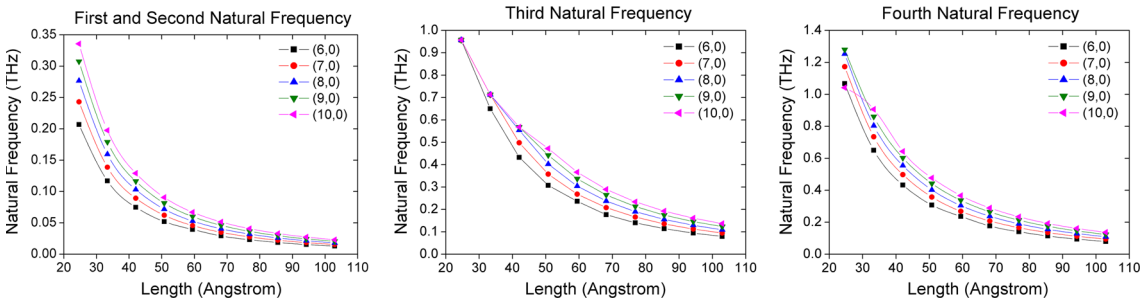

Fig. 8 First four natural frequencies of clamped-free zigzag SWCNTs of different length

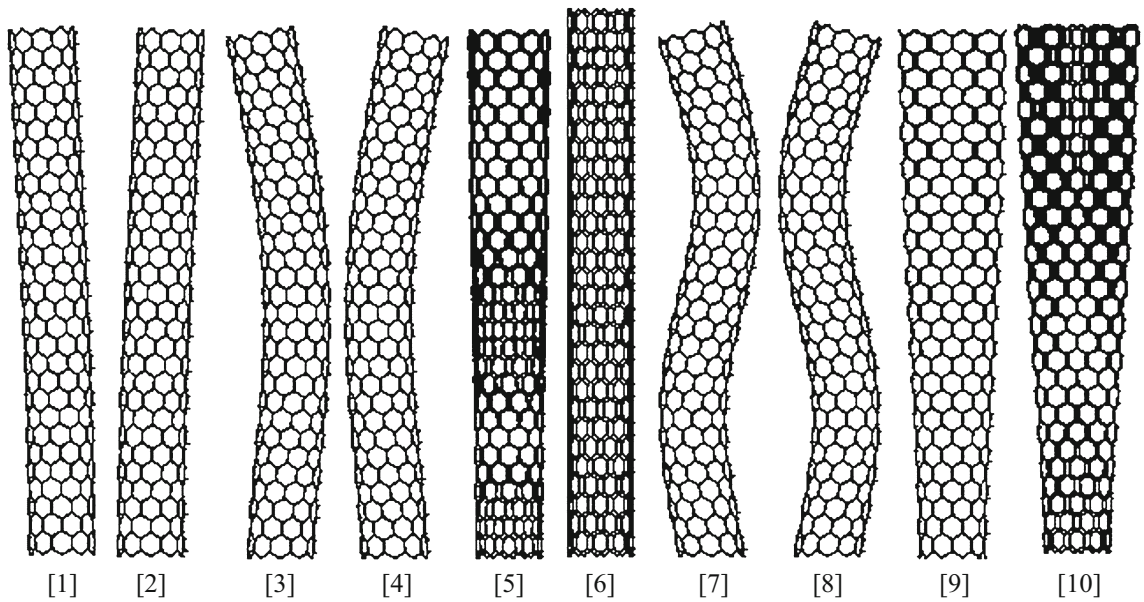

Fig. 9 First ten mode shapes of the (10, 0) zigzag SWCNT with a clamped-free boundary condition

The fundamental natural frequency of the nanotube decreases with the increase in length, and this is due to the fact that the number of carbon atoms increases, which increases the overall mass of the carbon nanotube. In this case, the addition of mass of carbon atoms dominates over the energy of carbon–carbon bonds, whereas if the diameter of nanotube increases without a change in the length, then the fundamental natural frequency also increases. In this case, the energy of carbon–carbon bonds dominates over the additional mass of carbon atoms. Both these phenomena can be clearly seen from Fig. 8.

It is also noticed that the difference in the values of natural frequencies decreases as the length of the nanotube increases and approaches each other at larger length. The frequency band of the fundamental natural frequency of shorter nanotubes (0.129 THz) is comparatively larger than of longer nanotubes (0.01 THz), as shown in Fig. 8. This can be very important statistics while selecting the length of the nanotube based on the required frequency band for its application in actual practice.

The study of modes of vibration is of equal importance for the corresponding resonant frequencies. Mode shapes contain the information of the nature of resonant frequencies and help to identify the overall vibration characteristics of the structure. A zigzag (10, 0) SWCNT is considered, and its first ten modes of vibration are plotted in Fig. 9. The diameter and length of the zigzag (10, 0) SWCNT are taken as 7.994 and 63.8 Å, respectively. The numbers inside the parentheses in Fig. 9 show the respective mode number, and this convention is followed in all the mode shape figures. The natural frequencies of these first ten modes are 0.059, 0.059, 0.325, 0.325, 0.377, 0.625, 0.794, 0.794, 1.019 and 1.019 THz, respectively. It is observed that there are three pairs of flexural modes, and each pair has the same natural frequency, but with different phase angle. These pairs of natural frequencies are the repeated roots of the characteristic equation of a zigzag SWCNT with clamped-free boundary condition.

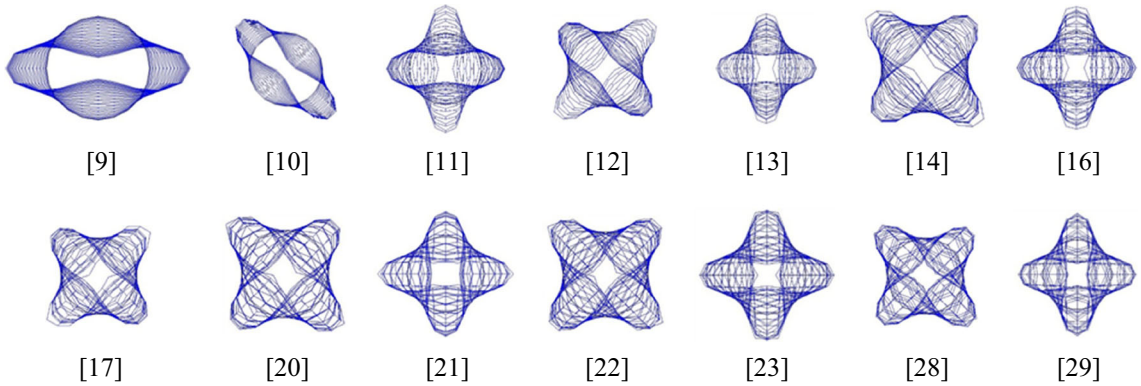

Fig. 10 Cross-section distortion mode shapes of the (10, 0) zigzag SWCNT with a clamped-free boundary condition

Modes 1–2 are the global flexural modes with same natural frequency. In these modes, all the carbon atoms exhibit displacements in one particular direction, globally. Similarly, modes 3–4 and 7–8 are also the other two pair of flexural modes. Modes 3–4 have the same natural frequency and modes 7–8 also have the same natural frequency, with different phase angle. In modes 3–4, the carbon atoms at the half-length of the tube exhibit maximum displacement compared to atoms at each end of the nanotube. Similarly, in modes 7–8, the carbon atoms near the half-length of the nanotube exhibit much less displacement and the atoms near one-fourth and three-fourth region experience maximum displacement. Mode 5 is the global torsion mode about the central axis of the nanotube. In this mode, all the carbon atoms exhibit displacement along the circumferential direction, except the atoms which are constrained in all directions near the fixed end. Mode 6 shows the global extensional behavior of the nanotube along its length. In this mode, the carbon atoms exhibit the displacement along the length of the nanotube. The term global mode of vibration is used to express the uncoupled modes of vibration, meaning that the flexural mode (modes 1–2) shows only the pure flexural behavior, and the torsion mode (mode 5) shows only the pure twisting of nanotube about its axis without any flexural and extensional effect. Modes 9 and 10 are the cross-section distortion modes with same natural frequencies. These modes are also the repeated eigenvalues of the characteristic equation of the zigzag SWCNT with clamped-free boundary condition.

Figure 10 shows the cross-section distortion modes of the zigzag (10, 0) SWCNT. These modes occur at high natural frequencies. From Figs. 9 and 10, it is observed that as the natural frequency of vibration increases, the sinusoidal wave forms along the axial and circumferential directions develop and become visible in the mode shapes. At higher natural frequencies, the cross-section of the nanotube becomes oval or gets distorted to accommodate the cross-sectional deformation as shown in Fig. 10. In Fig. 10, modes 9 and 10 are the radial breathing modes with same natural frequency, but with different phase angle. To understand and visualize the higher modes of vibration associated with sinusoidal circumferential and axial wave form, the cross-section distortion modes of the zigzag (10, 0) SWCNT with a clamped-free boundary condition are shown in Fig. 10.

4.1.2 Clamped–clamped zigzag SWCNTs

Figure 11 shows the variation of first four natural frequencies of zigzag SWCNTs with respect to the length, for clamped–clamped boundary condition. The first and second natural frequencies are the repeated eigenvalues of the characteristic equation of zigzag SWCNTs. From Fig. 11, it is observed that all the natural frequencies decrease with the increase in length of the nanotube, as observed in the case of clamped-free boundary condition. The rate of decrease in natural frequencies is larger near the smaller length and becomes smaller with the increase in length. The frequency band of the fundamental natural frequency of shorter nanotubes (0.205 THz) is comparatively larger than for longer nanotubes (0.06 THz), as shown in Fig. 11.

The zigzag SWCNTs with a clamped–clamped boundary condition show a higher fundamental natural frequency compared to clamped-free boundary condition. This is due to the fact that the stiffness of the nanotube at both extreme ends get enhanced due to enforcement of the constraint condition on those carbon atoms. From Figs. 9 and 11, it is observed that the nanotube (6, 0) shows different behavior in the third natural frequency compared to other nanotubes, viz. (7, 0), (8, 0), (9, 0) and (10, 0). The difference in the values of natural frequencies of nanotube (6, 0) with the nanotubes of other chirality is very samll in case of clamped-

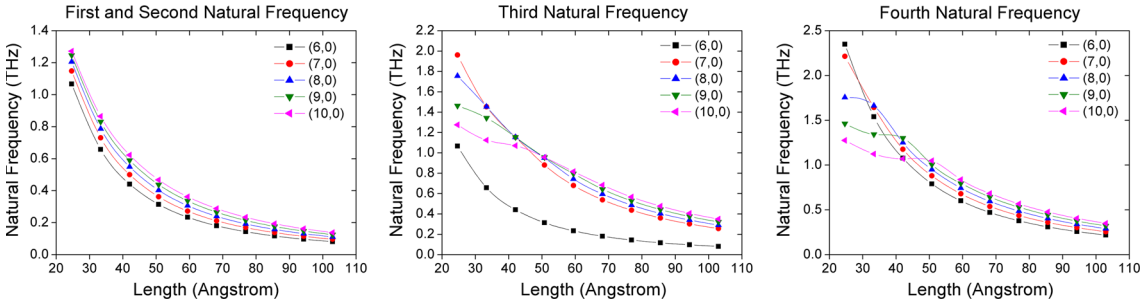

Fig. 11 First four natural frequencies of clamped–clamped zigzag SWCNTs of different length

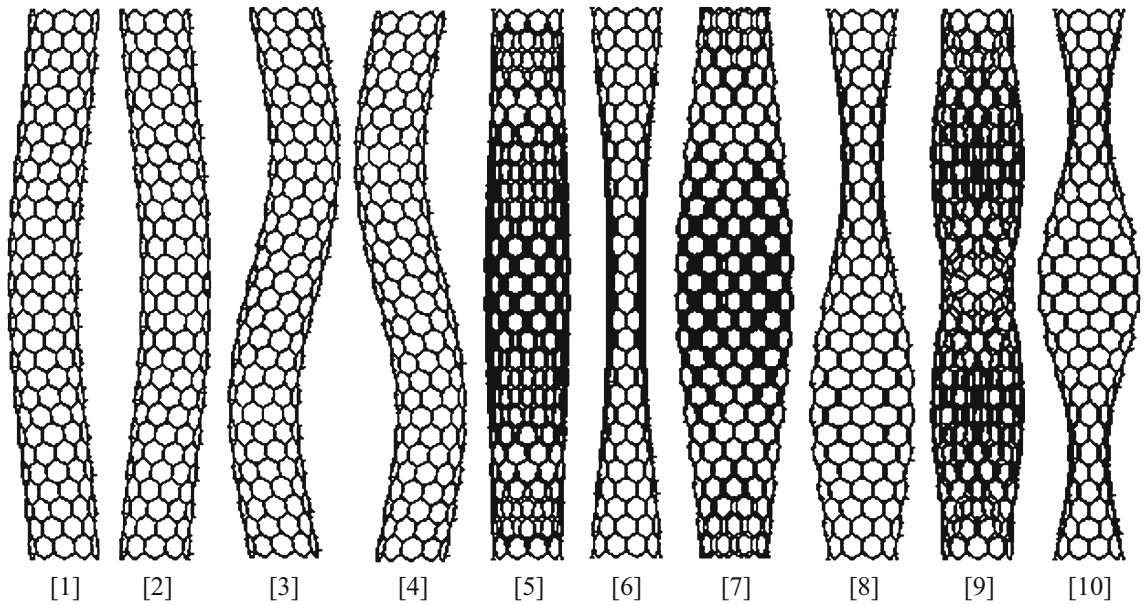

Fig. 12 First ten mode shapes of the (10, 0) zigzag SWCNT with a clamped–clamped boundary condition

free boundary condition (Fig. 9), whereas this difference is significant in case of clamped–clamped boundary condition (Fig. 11). For 24.65 Å length, the fourth natural frequency of only (10, 0) nanotube is less than (6, 0) nanotube for clamped-free boundary condition (Fig. 9), whereas for clamped–clamped boundary condition, the fourth natural frequency of nanotubes (7, 0), (8, 0), (9, 0) and (10, 0) is less than that of nanotube (6, 0), as shown in Fig. 11. This reduction in frequency is due to the reason that cross-sectional deformation is playing a major part in these tube modes. As diameter of the tube increases, it becomes easier to deform the tube section giving it a shell-type deformation pattern. This shows the different behavior of same nanotubes for different boundary conditions.

A zigzag (10, 0) SWCNT with the same specification, as mentioned in clamped-free boundary condition is considered, and its first ten modes of vibration are plotted in Fig. 12 for clamped–clamped boundary condition. The natural frequencies associated with the first ten modes are 0.322, 0.322, 0.755, 0.755, 0.762, 1.034, 1.034, 1.099, 1.099 and 1.242 THz, respectively. It is observed that there are four pairs of modes in the first ten natural frequencies, and each pair has the same natural frequency, but with the different phase angle. These pairs of natural frequencies are the repeated roots of the characteristic equation of zigzag SWCNT with clamped–clamped boundary condition. The discussion of mode shapes in case of clamped-free boundary condition is valid for the case of clamped–clamped boundary condition also. In Fig. 12, modes 1–2 are the flexural modes with same natural frequency. In these modes, the carbon atoms at the half-length of the nanotubes exhibit maximum displacement in transverse direction and form half-sine waves. Similarly, modes 3–4 are also the other pair of flexural modes and form the full-sine wave. In modes 3–4, the carbon atoms near the half-length of the nanotube exhibit very small displacement and the atoms near one-fourth and three-fourth region experience maximum displacement. Mode 5 is the torsion mode about the central axis of the nanotube.

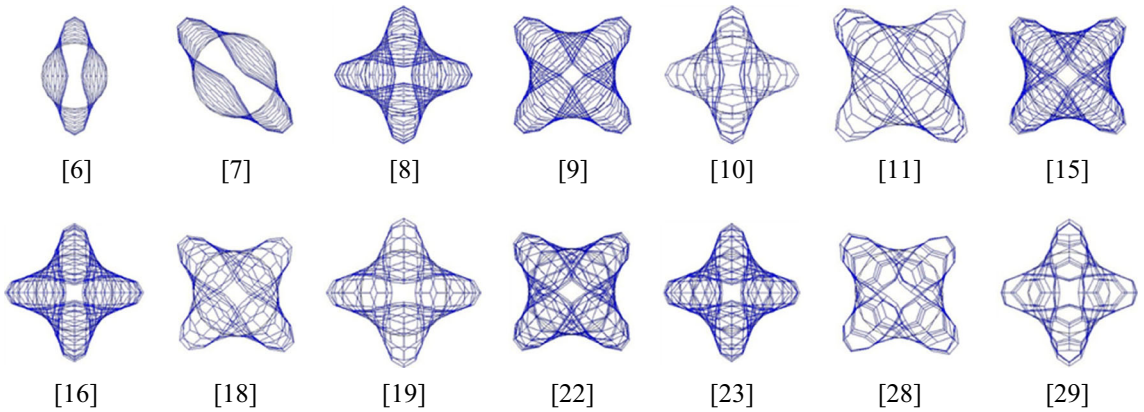

Fig. 13 Cross-section distortion mode shapes of the (10, 0) zigzag SWCNT with a clamped–clamped boundary condition

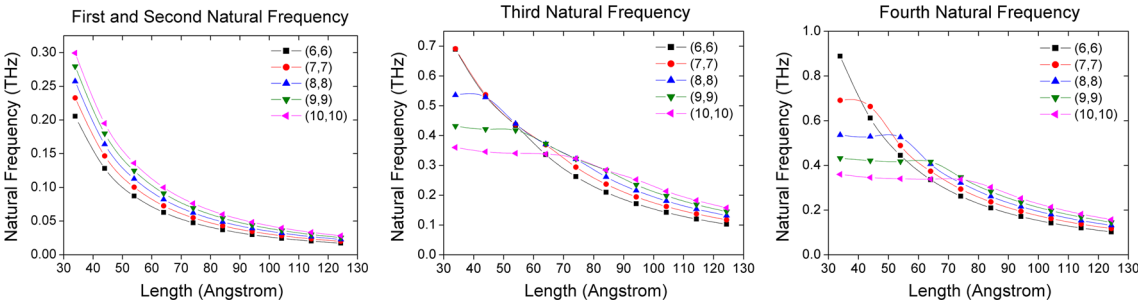

Fig. 14 First four natural frequencies of clamped-free armchair SWCNTs of different length

In this mode, all the carbon atoms exhibit displacement along the circumferential direction, except the atoms which are constrained in all directions near both the ends. Modes 6–7 are the radial breathing displacement modes with same natural frequency and different phase angle. Modes 8–9 are the cross-section distortion modes with repeated eigenvalues and different phase angle, as shown in Figs. 12 and 13.

Figure 13 shows the higher-order cross-section distortion modes of the zigzag (10, 0) SWCNT with a clamped–clamped boundary condition. The axial sinusoidal waveform is clearly visible in modes 8–10 (Figs. 12, 13). To understand and visualize the other higher modes of vibration associated with sinusoidal circumferential and axial wave form, the cross-section distortion modes of the zigzag (10, 0) SWCNT with a clamped–clamped boundary condition are shown in Fig. 13.

4.1.3 Clamped-free armchair SWCNTs

In this section, the vibration characteristics of armchair SWCNTs are presented. Figure 14 shows the variation of the first four natural frequencies of armchair SWCNTs with respect to the length, for clamped-free boundary condition. The general trends of repeated eigenvalues, gradual decrease in natural frequencies and frequency values coming closer at larger lengths are similar to those discussed for zigzag nanotubes. The third natural frequency of nanotubes (6, 6) and (7, 7) are nearly coinciding with each other for the length of 33.905 Å. The detailed explanation of all the observed phenomena is the same as discussed in the case of zigzag clamped-free boundary condition.

An armchair (5, 5) SWCNT is considered, and its first ten vibration modes are studied. These modes are plotted in Fig. 15. The diameter and length of the armchair (5, 5) SWCNT are taken as 6.923 and 61.5311 Å, respectively. The natural frequencies of these first ten modes are 0.057, 0.057, 0.314, 0.314, 0.376, 0.664, 0.759, 0.759, 1.128 and 1.276 THz, respectively. From Fig. 15, it is observed that there are three pairs of flexural modes, and each pair has the same natural frequency (repeated roots), but with different phase angle. Similar pairs are also observed in zigzag SWCNTs. Modes 1–8 shows the similar pattern of vibration as observed in the case of the zigzag (10, 0) SWCNT with clamped-free boundary condition (Fig. 9). The observations and explanations of these modes are the same as discussed earlier. Mode 9 is the second torsion mode with two

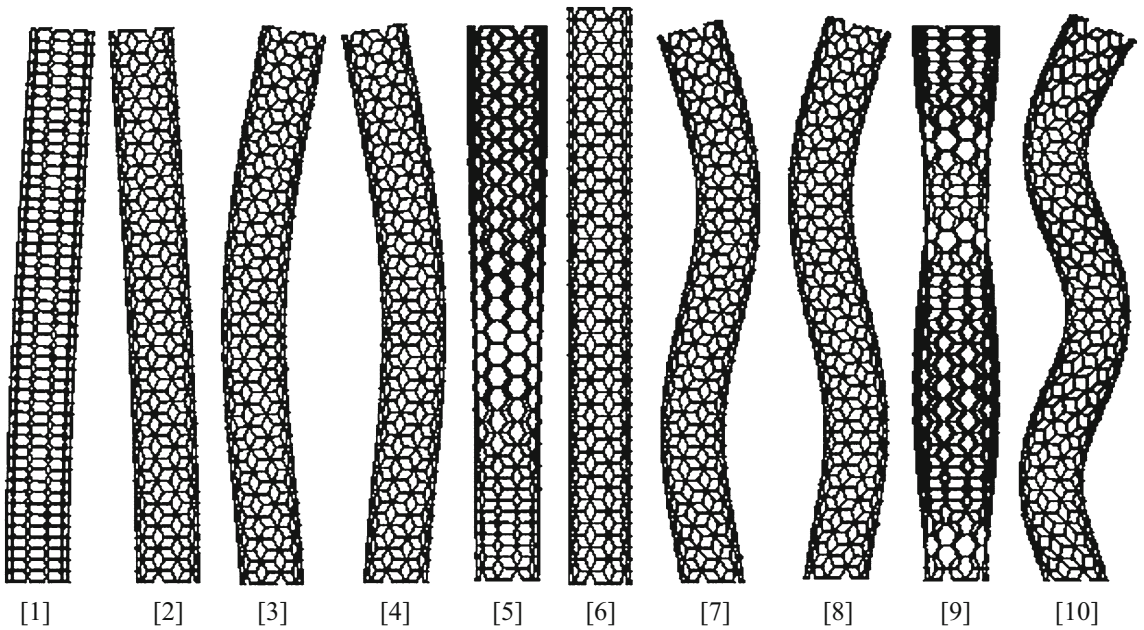

Fig. 15 First ten mode shapes of the (5, 5) armchair SWCNT with a clamped-free boundary condition

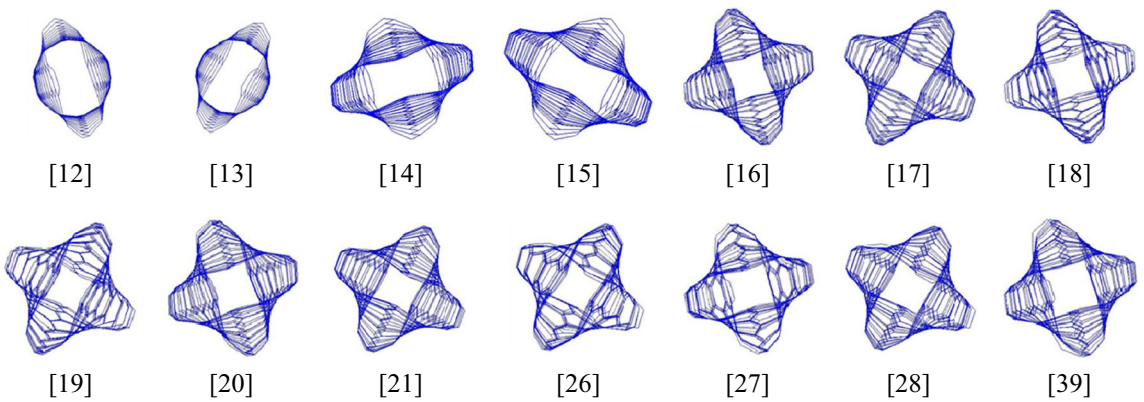

Fig. 16 Cross-section distortion mode shapes of the (5, 5) armchair SWCNT with a clamped-free boundary condition

nodes where the carbon atoms exhibit zero displacement. The first torsion mode is the fifth mode with only a single node positioned at the fixed end of the nanotube. Mode 10 is the higher-order flexure mode. The modes 9–10 are the extra modes which are not present in the first ten modes of the zigzag (10, 0) SWCNT.

Figure 16 shows the cross-section distortion modes of the armchair (5, 5) SWCNT with a clamped-free boundary condition. These mode shapes play a very important role to understand and visualize the higher modes of vibration associated with sinusoidal circumferential and axial wave form.

4.1.4 Clamped–clamped armchair SWCNTs

Figure 17 shows the variation of first four natural frequencies of armchair SWCNTs with respect to the length, for clamped–clamped boundary condition. The frequency band of the fundamental natural frequency of the shorter nanotube is 0.205 THz, whereas for longer nanotubes it is 0.052 THz, as shown in Fig. 17. The armchair SWCNTs with a clamped–clamped boundary condition shows the higher fundamental natural frequency compared to clamped-free boundary condition. Also, the resonant frequency pattern of armchair SWCNTs with clamped–clamped boundary condition is entirely different than observed in clamped-free conditions.

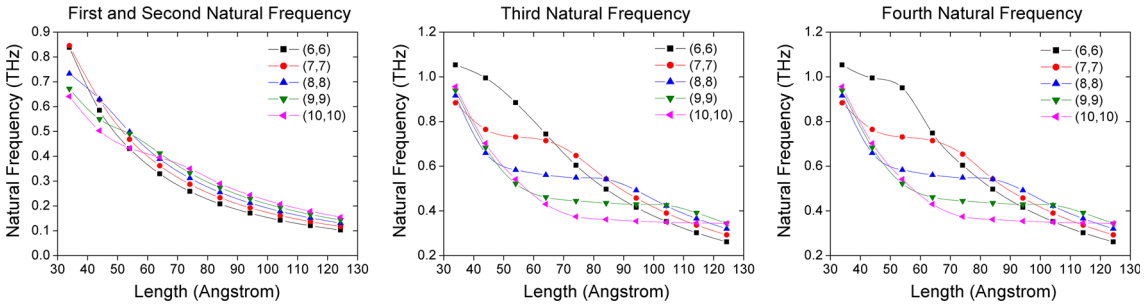

Fig. 17 First four natural frequencies of clamped–clamped armchair SWCNTs of different length

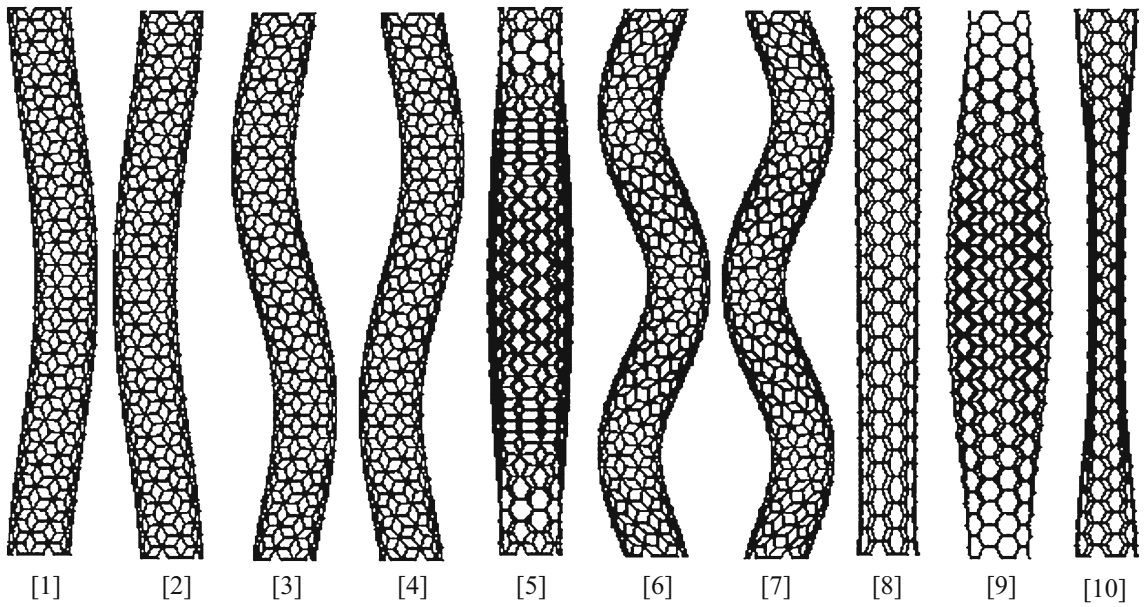

Fig. 18 First ten mode shapes of the (5, 5) armchair SWCNT with a clamped–clamped boundary condition

An armchair (5, 5) SWCNT with the same specification as mentioned earlier in armchair clamped-free boundary condition is considered, and its first ten modes of vibration are plotted in Fig. 18 for clamped–clamped boundary condition. The natural frequencies of these first ten modes are 0.310, 0.310, 0.721, 0.721, 0.765, 1.215, 1.215, 1.342, 1.377 and 1.377 THz, respectively. From Fig. 18, it is observed that there are four pairs of modes in first ten natural frequencies, and each pair has the same natural frequency, but with the different phase angle. Modes 1–5 shows the similar pattern of vibration as observed in the case of the zigzag (10, 0) SWCNT with a clamped-free boundary condition. The observations and explanations of these modes are the same as discussed earlier. Mode 8 is the extensional mode of vibration where the carbon atoms exhibit displacement along the length of the tube. Modes 9–10 are the radial breathing displacement modes with same natural frequency and different phase angle. Figure 19 shows the cross-section distortion modes of the armchair (5, 5) SWCNT with a clamped–clamped boundary condition.

4.2 Dependence on the diameter

In this section, the dependence of natural frequencies of armchair and zigzag SWCNTs on their diameter are investigated for clamped-free and clamped–clamped boundary conditions. While computing the resonant frequencies of armchair and zigzag SWCNTs with different diameters, the length of the nanotube is kept constant at 61.53 and 63.8 Å, respectively. The variations of the first three natural frequencies with respect to the diameter are shown in Fig. 20 for respective conditions. In armchair nanotubes with clamped-free boundary condition, the fundamental frequency increases with an increase in diameter, whereas the third natural frequency first increases and then decreases. The same nanotube for clamped–clamped boundary

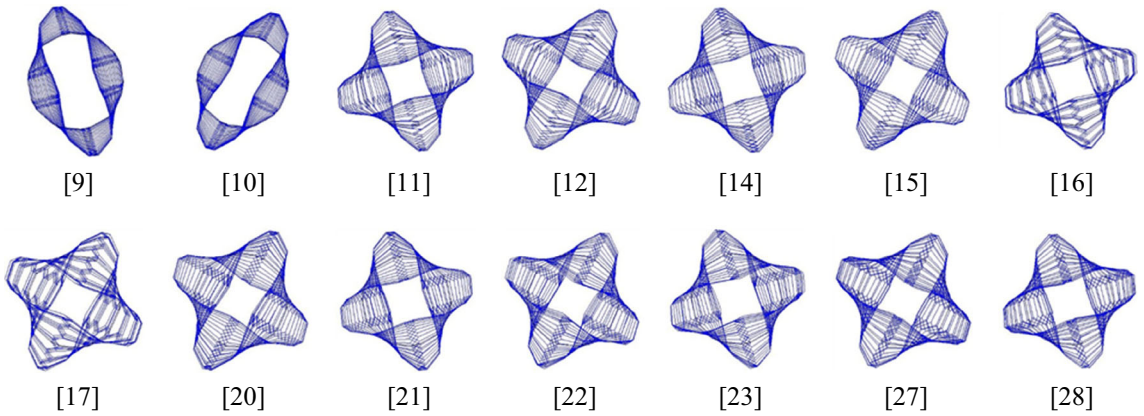

Fig. 19 Cross-section distortion mode shapes of the (5, 5) armchair SWCNT with a clamped–clamped boundary condition

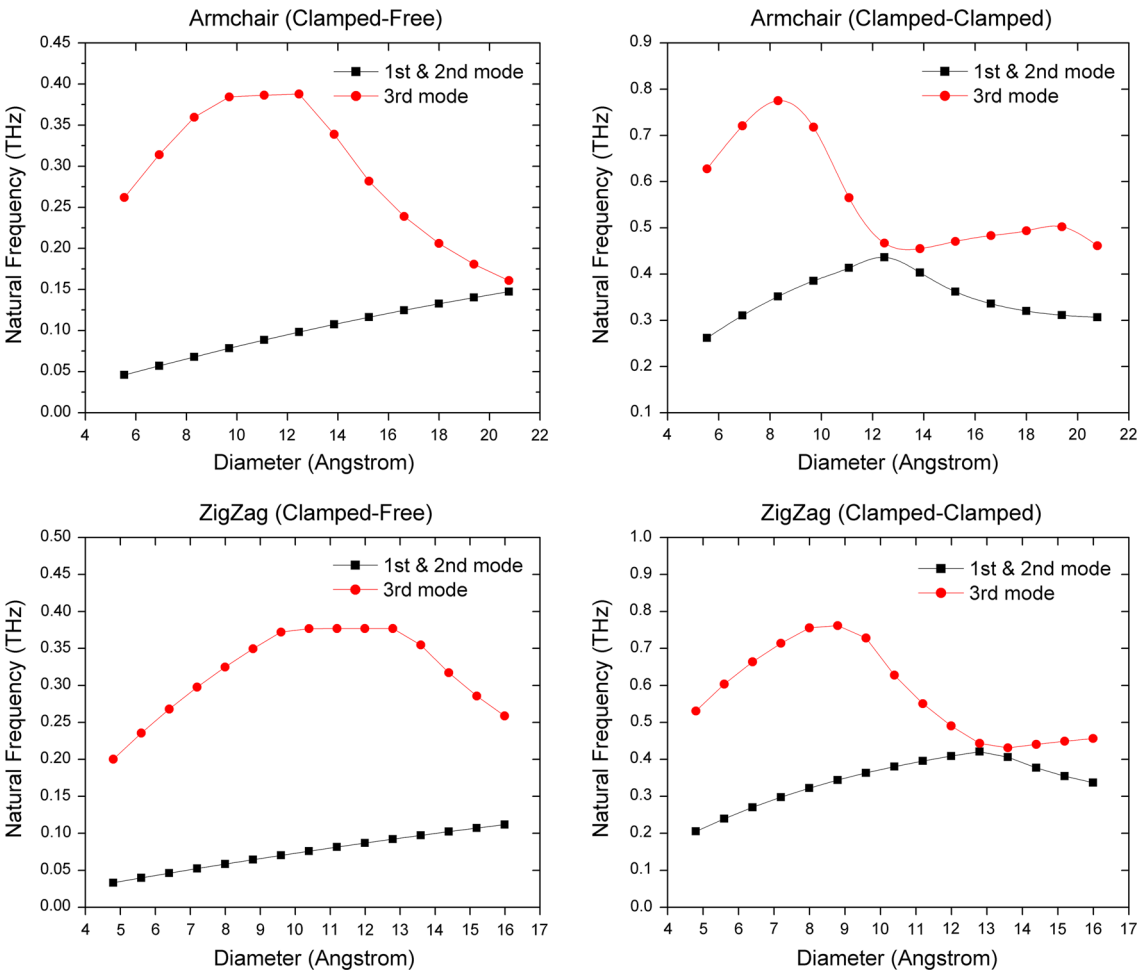

Fig. 20 Variation of first three natural frequencies of armchair and zigzag SWCNTs of different diameters for clamped-free and clamped–clamped boundary condition

condition shows different behavior. In this case, the fundamental frequency first increases with an increase in diameter and then decreases, whereas the third natural frequency initially increases and then decreases and again start increasing. A similar trend of variation in natural frequencies is also observed for zigzag SWCNT, as shown in Fig. 20. The decrease in the natural frequency of nanotube with an increase in diameter is due to the fact that the additional mass of carbon atoms dominates over the energy of the carbon–carbon bonds

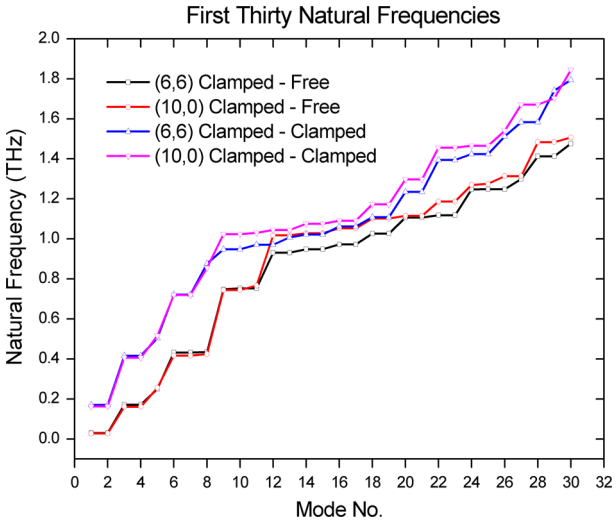

Fig. 21 First thirty natural frequencies of armchair and zigzag SWCNTs with clamped-free and clamped–clamped boundary condition

(stiffness), whereas the increase in natural frequency with an increase in diameter is because the energy of the carbon–carbon bonds dominates over the additional mass of carbon atoms.

4.3 Dependence on atomic structure

In the previous discussion, it has been observed that armchair and zigzag SWCNTs show very similar vibration characteristics only at the lower modes of vibration, whereas at very high resonant frequencies, these nanotubes show different dynamic behavior. This behavior is investigated in this section in more detail. Figure 21 shows the first thirty natural frequencies of armchair (6, 6) and zigzag (10, 0) SWCNTs for clamped-free and clamped–clamped boundary conditions. The combination of carbon nanotubes (6, 6) and (10, 0) are selected such that the diameter of both the nanotubes is same, to see the influence of atomic structure on its vibration characteristics. The length of armchair and zigzag SWCNT is taken as 61.53 and 63.8 Å, respectively. Figure 21 shows that the natural frequency of armchair (6, 6) SWCNT is significantly lower than the zigzag (10, 0) SWCNT at higher modes of vibration for both clamped-free and clamped–clamped boundary conditions. This is due to the fact that the number of carbon atoms in armchair nanotube is more compared to zigzag nanotube for the approximately same diameter. This additional mass of carbon atoms becomes significant and dominates over the energy between carbon–carbon bonds at higher modes of vibration.

4.4 Capped single-walled carbon nanotubes

The vibration characteristics of capped armchair and capped zigzag SWCNTs are investigated in this section and compared with the open-end SWCNTs of same chirality. Three capped armchair nanotubes, i.e., (5, 5), (6, 6) and (10, 10), and two capped zigzag nanotubes, i.e., (9, 0) and (10, 0), with clamped-free and clamped–clamped boundary conditions are considered. The length of a capped armchair and capped zigzag nanotubes is taken as 69.29 and 67.23 Å, respectively.

4.4.1 Capped armchair SWCNTs

Figure 22 shows the comparison of first ten natural frequencies of open- and capped-end armchair SWCNTs for clamped-free and clamped–clamped boundary conditions. The atoms considered as clamped in case of capped nanotube are shown in Fig. 22. Capped armchair nanotubes show considerable lower natural frequencies compared to the open-end configuration. This is due to the extra mass of additional carbon atoms at the capped portion of nanotubes and an increase in the overall length of the nanotube by the addition of capped structure.

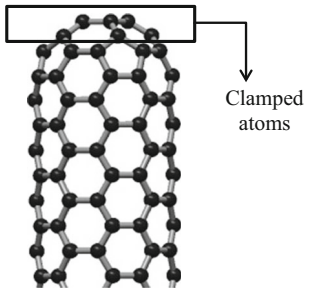

Fig. 22 Clamped atoms in capped nanotube

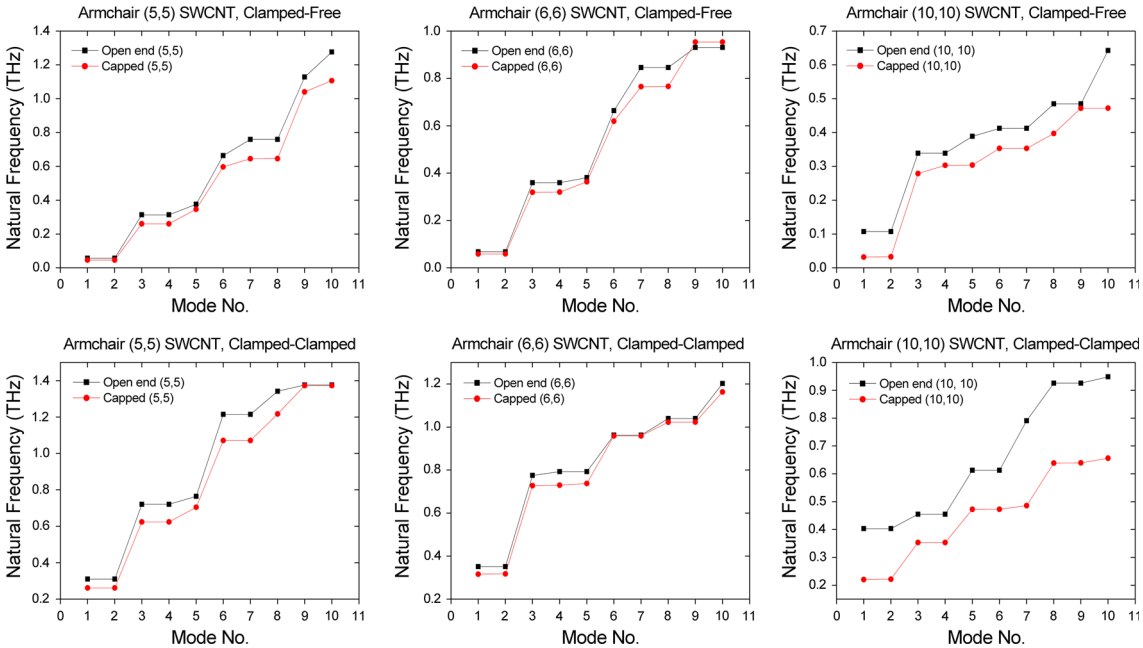

Fig. 23 First ten natural frequencies of open- and capped-end armchair SWCNTs for clamped-free and clamped–clamped boundary conditions

It is observed that the difference in frequency values of capped- and open-end armchair nanotubes is less for smaller diameter nanotubes, i.e., (5, 5) and (6, 6), whereas for larger diameter nanotube, i.e., (10, 10), the difference is significant and needs attention while selecting these nanotubes in actual use. From Fig. 23 and exact numerical values, it is also observed that the repeated eigenvalues of capped-end nanotubes are not exactly the same. Some deviation in the frequency values of repeated roots of the characteristic equation is found. The possible reason for this deviation may be due to the disturbance in symmetry of the nanotube by the addition of a capped structure.

Figure 24 shows the first ten mode shapes of armchair (5, 5) SWCNT for clamped-free boundary condition. The frequencies associated with these modes are 0.0463, 0.0463, 0.2609, 0.2609, 0.3469, 0.5972, 0.6457, 0.6457, 1.0406 and 1.107 THz, respectively, whereas Fig. 25 shows the first ten mode shapes of armchair (5, 5) SWCNT for clamped–clamped boundary condition. The frequencies associated with these modes are 0.2619, 0.2619, 0.6241, 0.6241, 0.7047, 1.0711, 1.0711, 1.2176, 1.3731 and 1.3731 THz, respectively. The capped armchair SWCNT with clamped-free and clamped–clamped boundary conditions shows the similar mode shapes as observed in open-end armchair SWCNT with same boundary condition. So, the observations derived from these mode shapes and their explanations are same as discussed in open-end armchair SWCNT (Figs. 15, 18).

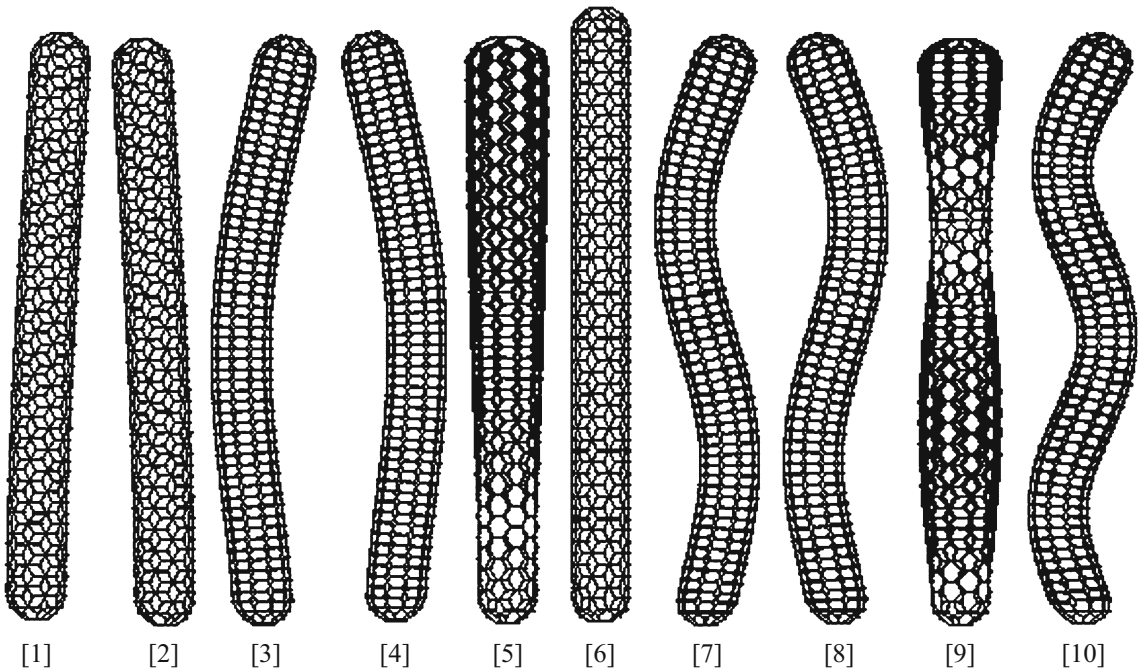

Fig. 24 First ten mode shapes of the (5, 5) capped armchair SWCNT with a clamped-free boundary condition

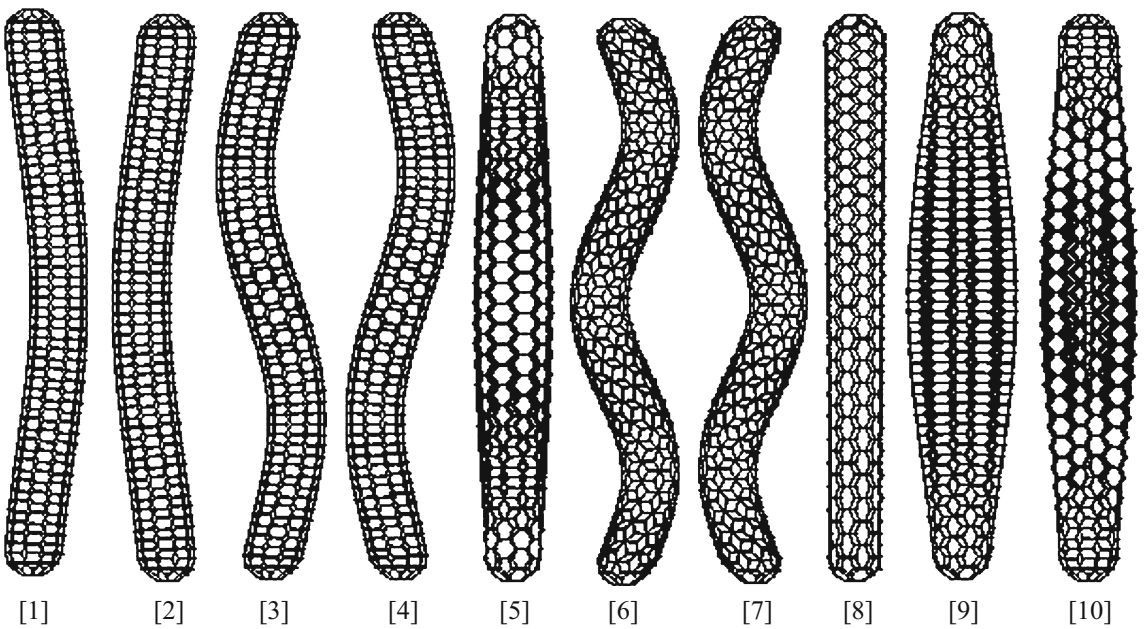

Fig. 25 First ten mode shapes of the (5, 5) capped armchair SWCNT with a clamped–clamped boundary condition

4.4.2 Capped zigzag SWCNTs

Figure 26 shows the comparison of first ten natural frequencies of open- and capped-end zigzag SWCNTs for clamped-free and clamped–clamped boundary conditions. A capped (9, 0) zigzag nanotube shows marginal lower natural frequencies compared to the open-end configuration, whereas the capped (10, 0) zigzag nanotube is seen to follow the same trend of resonant frequencies as the (10, 0) open-end zigzag nanotube. Some deviation in the frequency values of repeated roots of the characteristic equation is found, similar to those observed in the case of capped armchair nanotubes.

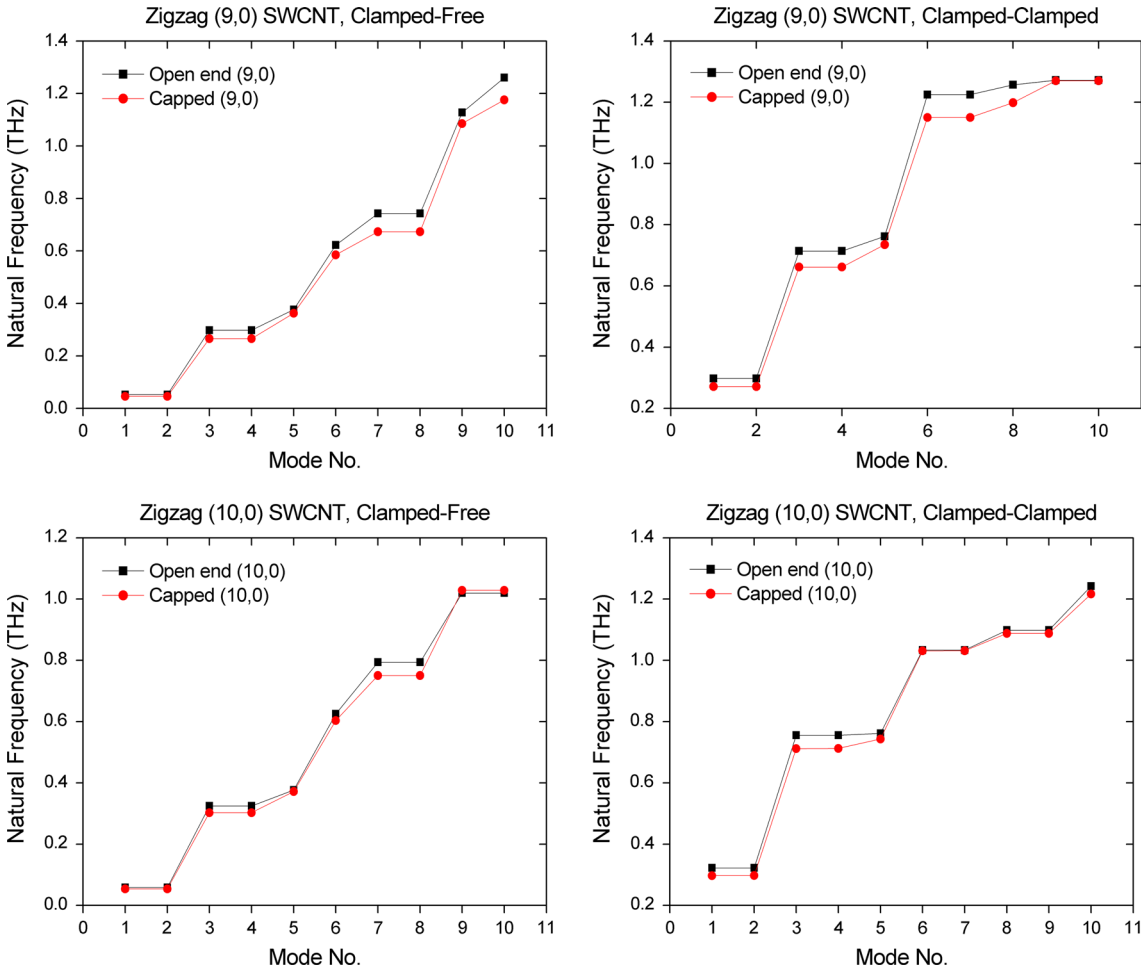

Fig. 26 First ten natural frequencies of open- and capped-end zigzag SWCNTs for clamped-free and clamped–clamped boundary conditions

Figure 27 shows the first ten mode shapes of zigzag (9, 0) SWCNT for clamped-free boundary condition. The frequencies associated with these modes are 0.0461, 0.0461, 0.2659, 0.2659, 0.3626, 0.5850, 0.6731, 0.6731, 1.0857 and 1.1759 THz, respectively, whereas Fig. 28 shows the first ten mode shapes of zigzag (9, 0) SWCNT for clamped–clamped boundary condition. The frequencies associated with these modes are 0.2713, 0.2713, 0.6615, 0.6615, 0.7347, 1.1506, 1.1506, 1.1986, 1.2702 and 1.2702 THz, respectively. From Fig. 27, it is observed that the capped (9, 0) zigzag SWCNT with a clamped-free boundary condition follows the mode shapes of open-end (5, 5) armchair SWCNT (Fig. 15) with same boundary condition. Also, from Fig. 28, it is observed that the capped (9, 0) zigzag SWCNT with a clamped–clamped boundary condition follows the mode shapes of open-end (5, 5) armchair SWCNT (Fig. 18) with same boundary condition. The observations derived from these mode shapes (Figs. 27, 28) and their explanations are same as discussed for open-end (5, 5) armchair SWCNT for respective boundary conditions (Figs. 15, 18).

5 Conclusions

A multi-scale AFEM incorporating multi-body interatomic TB potential is presented in this paper, and the vibration characteristics of open- and capped-end armchair and zigzag SWCNTs subjected to clamped-free and clamped–clamped boundary conditions are investigated. Space frame and three-dimensional mass elements are used in this method to represent carbon–carbon bond and carbon atom, respectively. The stretching stiffness and bond angle bending stiffness parameters are derived from TB potential, and a new set of force constant parameters is established. Structural and molecular mechanics analogy is used along with new set of force

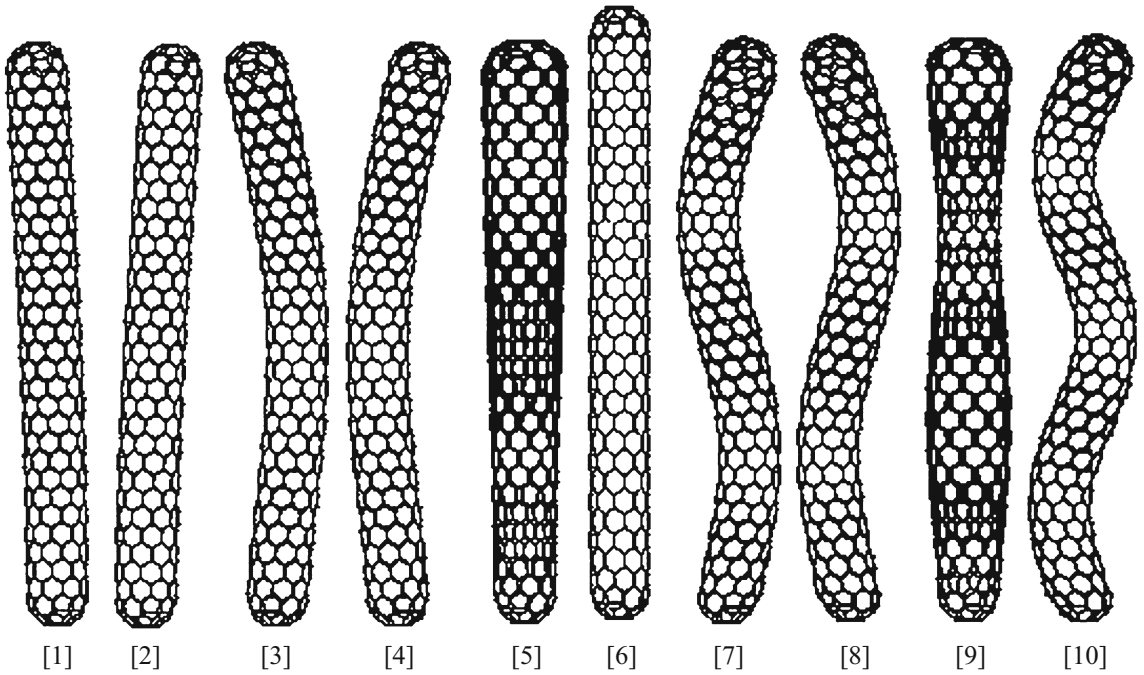

Fig. 27 First ten mode shapes of the (9, 0) capped zigzag SWCNT with a clamped-free boundary condition

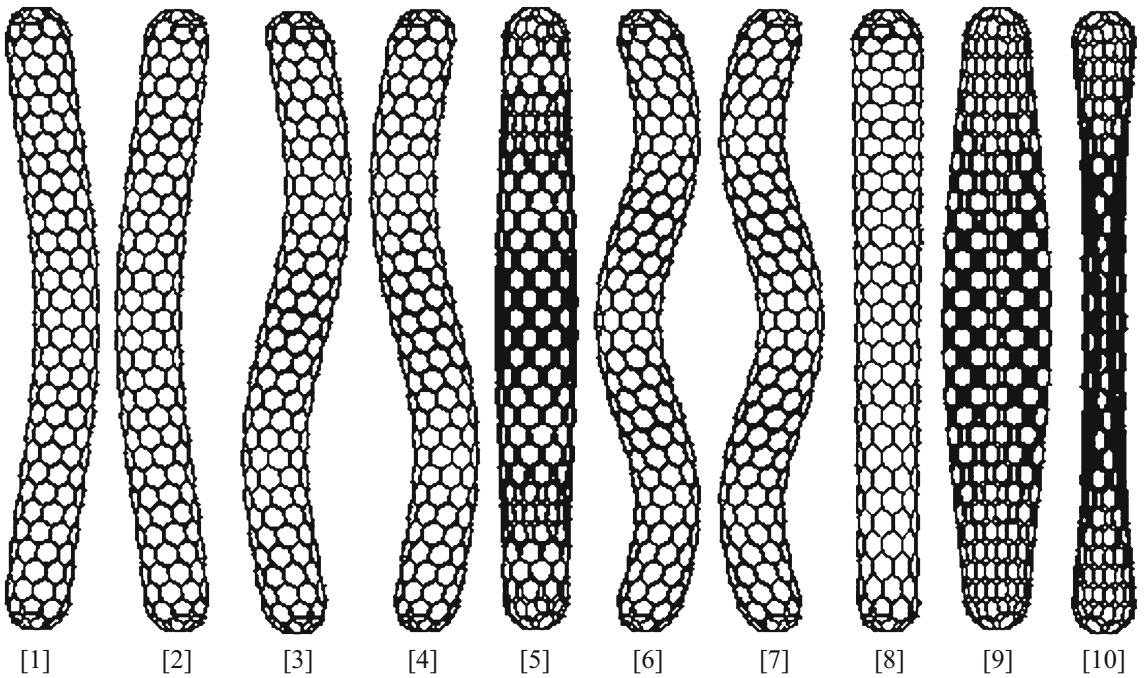

Fig. 28 First ten mode shapes of the (9, 0) capped zigzag SWCNT with a clamped–clamped boundary condition

constants to compute the equivalent geometric and elastic properties of the space frame element which are consistent with material constitutive relations, to represent a carbon–carbon bond. The model used to find the dynamic behavior of SWCNTs is also validated by comparing the results of frequencies from MD simulation and the available results in the literature. The values of frequencies from MD simulation and the proposed AFEM are in good agreement with each other. Also, the proposed method predicts the frequency values better as compared to the results available in the literature.

The vibration characteristics of open-end zigzag and armchair SWCNTs are investigated, and its dependence on length, diameter and atomic structure of the SWCNTs is studied. It is observed that the first and second eigenvalues of SWCNTs are repeated roots of the characteristic equation and show the similar mode shape with different phase angle. For all chirality of SWCNTs with clamped-free and clamped–clamped boundary conditions, all of the natural frequencies decrease with the increase in the length of the nanotube. The computed results also show that the rate of decrease in natural frequencies is larger near the lower length and becomes smaller with the increase in length. It is also found that the difference in the values of respective natural frequencies of different nanotubes decreases as the length increases and approaches to each other at larger length. The frequency band of fundamental natural frequency of shorter SWCNTs is comparatively larger than longer SWCNTs, and this is very important statistics while selecting the length of SWCNTs based on the required frequency band for its application.

It is observed that the armchair and zigzag SWCNTs show very similar vibration characteristics only at the lower modes of vibration, but at very high resonant frequencies, these nanotubes show different dynamic behavior. At higher modes of vibration, the zigzag SWCNTs show significantly larger values of natural frequencies compared to armchair SWCNTs of approximate same diameter. From the mode shapes of the SWCNTs, it is observed that as the natural frequency of vibration increases, the mode shapes involve more of cross-sectional deformation. It is observed that the capped-end SWCNTs vibrate at a comparatively lower natural frequency than in an open-end configuration though the modes of vibrations are the same. The difference in frequency values is less for smaller diameter nanotubes, but for larger diameter the difference is significant. The additional capped structures disturb the symmetry of nanotubes, and so the repeated eigenvalues are slightly deviating from each other. The investigated vibration characteristics of SWCNTs using proposed AFEM are very important findings and may be very helpful while designing nanoresonators, actuators and nanoelectromechanical devices. Also, the procedure and numerical model established in this paper can be used further for other nanostructures to investigate their overall static and dynamic characteristics.

References

1. Poncharal, P., Wang, Z.L., Ugarte, D., De Heer, W.A.: Electrostatic deflections and electromechanical resonances of carbon nanotubes. Science **283**(5407), 1513–1516 (1999)
2. Shen, L., Li, J.: Transversely isotropic elastic properties of single-walled carbon nanotubes. Phys. Rev. B Condensed Matter Mater. Phys. **69**(4), 454141–4541410 (2004)
3. Shen, L., Li, J.: Transversely isotropic elastic properties of multiwalled carbon nanotubes. Phys. Rev. B Condensed Matter Mater. Phys. 71(3) (2005). doi:10.1103/PhysRevB.71.035412
4. Shen, L., Li, J.: Equilibrium structure and strain energy of single-walled carbon nanotubes. Phys. Rev. B Condensed Matter Mater. Phys. 71(16) (2005). doi:10.1103/PhysRevB.71.165427
5. Wang, C.M., Tan, V.B.C., Zhang, Y.Y.: Timoshenko beam model for vibration analysis of multi-walled carbon nanotubes. J. Sound Vib. **294**(4), 1060–1072 (2006)
6. Sun, C., Liu, K.: Vibration of multi-walled carbon nanotubes with initial axial loading. Solid State Commun. **143**(4–5), 202–207 (2007)
7. Gupta, S.S., Batra, R.C.: Continuum structures equivalent in normal mode vibrations to single-walled carbon nanotubes. Comput. Mater. Sci. **43**(4), 715–723 (2008)
8. Georgantzinos, S.K., Giannopoulos, G.I., Anifantis, N.K.: An efficient numerical model for vibration analysis of single-walled carbon nanotubes. Comput. Mech. **43**(6), 731–741 (2009)
9. Georgantzinos, S.K., Anifantis, N.K.: Vibration analysis of multi-walled carbon nanotubes using a spring-mass based finite element model. Comput. Mater. Sci. **47**(1), 168–177 (2009)
10. Ke, L.L., Xiang, Y., Yang, J., Kitipornchai, S.: Nonlinear free vibration of embedded double-walled carbon nanotubes based on nonlocal Timoshenko beam theory. Comput. Mater. Sci. **47**(2), 409–417 (2009)
11. Sakhaee-Pour, A., Ahmadian, M.T., Vafai, A.: Vibrational analysis of single-walled carbon nanotubes using beam element. Thin-Walled Struct. **47**(6-7), 646–652 (2009)
12. Chowdhury, R., Adhikari, S., Wang, C.Y., Scarpa, F.: A molecular mechanics approach for the vibration of single-walled carbon nanotubes. Comput. Mater. Sci. **48**(4), 730–735 (2010)
13. Arghavan, S., Singh, A.V.: On the vibrations of single-walled carbon nanotubes. J. Sound Vib. **330**(13), 3102–3122 (2011)
14. Aydogdu, M.: Axial vibration analysis of nanorods (carbon nanotubes) embedded in an elastic medium using nonlocal elasticity. Mech. Res. Commun. **43**, 34–40 (2012)
15. Ansari, R., Gholami, R., Rouhi, H.: Vibration analysis of single-walled carbon nanotubes using different gradient elasticity theories. Compos. B Eng. **43**(8), 2985–2989 (2012)
16. Ghavanloo, E., Fazelzadeh, S.A.: Vibration characteristics of single-walled carbon nanotubes based on an anisotropic elastic shell model including chirality effect. Appl. Math. Model. **36**(10), 4988–5000 (2012)

17. Cornell, W.D., Cieplak, P., Bayly, C.I., Gould, I.R., Merz, K.M. Jr., Ferguson, D.M., Spellmeyer, D.C., Fox, T., Caldwell, J.W., Kollman, P.A.: A second generation force field for the simulation of proteins, nucleic acids, and organic molecules. J. Am. Chem. Soc. **117**(19), 5179–5197 (1995)
18. Tersoff, J.: Empirical interatomic potential for carbon, with applications to amorphous carbon. Phys. Rev. Lett. **61**(25), 2879–2882 (1988)
19. Brenner, D.W.: Empirical potential for hydrocarbons for use in simulating the chemical vapor deposition of diamond films. Phys. Rev. B **42**(15), 9458–9471 (1990)
20. Lee, J.H., Lee, B.S.: Modal analysis of carbon nanotubes and nanocones using FEM. Comput. Mater. Sci. **51**(1), 30–42 (2012). doi:10.1016/j.commatsci.2011.06.041
21. Li, C., Chou, T.W.: A structural mechanics approach for the analysis of carbon nanotubes. Int. J. Solids Struct. **40**(10), 2487–2499 (2003)
22. Rappé, A.K., Casewit, C.J., Colwell, K.S., Goddard Iii, W.A. Skiff W.M.: UFF, a full periodic table force field for molecular mechanics and molecular dynamics simulations. J. Am. Chem. Soc. **114**(25), 10024–10035 (1992)
23. Chang, T., Gao, H.: Size-dependent elastic properties of a single-walled carbon nanotube via a molecular mechanics model. J. Mech. Phys. Solids **51**(6), 1059–1074 (2003)
24. Gelin, B.R.: Molecular Modeling of Polymer Structures and Properties. Hanser/Gardner Publishers, Cincinnati (1994)
25. Gajbhiye, S.O., Singh, S.P.: Multiscale nonlinear frequency response analysis of single-layered graphene sheet under impulse and harmonic excitation using the atomistic finite element method. J. Phys. D Appl. Phys. **48**(14), 1–16 (2015). doi:10.1088/0022-3727/48/14/145305
26. Ye, L.H., Liu, B.G., Wang, D.S.: Ab initio molecular dynamics study on small carbon nanotubes. Chin. Phys. Lett. **18**(11), 1496–1499 (2001)
27. Scarpa, F., Adhikari, S.: A mechanical equivalence for Poisson's ratio and thickness of C–C bonds in single wall carbon nanotubes. J. Phys. D Appl. Phys. **41**(8), 1–5 (2008)
28. Gajbhiye, S.O., Singh, S.P.: Multiscale analysis approach to find the dynamic characteristics of graphene sheet. Appl. Mech. Mater. **592**(594), 1119–1124 (2014). doi:10.4028/www.scientific.net/AMM.592-594.1119
29. Gajbhiye, S.O., Singh, S.P.: A review of methodologies to multiscale modeling of nanostructures and nanocomposites. In: International Conference on Functional Materials (ICFM-2014), Materials Science Centre, Indian Institute of Technology, Kharagpur, India, p. 189. 5–7 Feb (2014)
30. Lu, X., Hu, Z.: Mechanical property evaluation of single-walled carbon nanotubes by finite element modeling. Compos. B Eng. **43**(4), 1902–1913 (2012). doi:10.1016/j.compositesb.2012.02.002
31. Fakhrabadi, M.M.S., Samadzadeh, M., Rastgoo, A., Yazdi, M.H., Mashhadi, M.M.: Vibrational analysis of carbon nanotubes using molecular mechanics and artificial neural network. Phys. E Low-Dimens. Syst. Nanostruct. **44**(3), 565–578 (2011). doi:10.1016/j.physe.2011.10.004
32. Sun, H., Ren, P., Fried, J.R.: The COMPASS force field: parameterization and validation for phosphazenes. Comput. Theor. Polym. Sci. **8**(1–2), 229–246 (1998). doi:10.1016/S1089-3156(98)00042-7